Metabolic evaluation of non-small cell lung cancer patient–derived xenografts models using ^{18}F-FDG PET: potential tools for early therapy response

Authors: Silvia Valtorta*(1,2), Massimo Moro*(3), Giovanna Prisinzano(1,4), Giulia Bertolini(3), Monica Tortoreto(5), Isabella Raccagni(2,4), Ugo Pastorino(6), Luca Roz§(3), Gabriella Sozzi#(3), Rosa Maria Moresco#§(2,4)

Affiliations: (1) Molecular Bioimaging and Physiology Institute (IBFM), National Researches Council (CNR), Segrate, Italy; (2) Medicine and Surgery Department and Tecnomed Foundation, University of Milano-Bicocca, Monza, Italy; (3) Tumor Genomics Unit, Experimental Oncology and Molecular Medicine Department, Fondazione IRCCS Istituto Nazionale dei Tumori, Milan, Italy; (4) Experimental Imaging Center, IRCCS San Raffaele Scientific Institute, Milan, Italy; (5) Molecular Pharmacology Unit, Experimental Oncology and Molecular Medicine Department, Fondazione IRCCS Istituto Nazionale dei Tumori, Milan, Italy; (6) Thoracic Surgery Unit, Surgery Department, Fondazione IRCCS Istituto Nazionale dei Tumori, Milan, Italy

* S. Valtorta and M. Moro equally contributed to this article

 # Joint senior authors

§ Corresponding authors:

Prof. Rosa Maria Moresco, University of Milano-Bicocca, Via Cadore 48, 20900 Monza (MB), Italy. Phone: +39-02-26433817; Fax: +39-02-2643-2717; e-mail: moresco.rosamaria@hsr.it

Luca Roz, Fondazione IRCCS Istituto Nazionale dei Tumori, Via Venezian 1, 20133 Milan, Italy. Phone: +39-02-23903775; Fax: +39-02-23902928; e-mail: luca.roz@istitutotumori.mi.it

First authors:

Silvia Valtorta, PhD, IBFM-CNR, Via F.lli Cervi 93, 20090 Segrate (MI), Italy. Phone: +39-02-26433640; Fax: +39-02-26432717; e-mail: valtorta.silvia@hsr.it

Massimo Moro, M.Sc., Fondazione IRCCS Istituto Nazionale dei Tumori, Via Venezian 1, 20133 Milan, Italy. Phone: +39-02-23903775; Fax: +39-02-23902928; e-mail: massimo.moro@istitutotumori.mi.it

Word count: 5000

Running title: Glucose metabolism in NSCLC PDX with PET

Keywords: ^{18}F-FDG PET, lung cancer, patient-derived xenograft, stem cells

ABSTRACT

Purpose: Lung cancer heterogeneity makes response to therapy extremely hard to predict. Patient-derived xenografts (PDXs) represent a reliable preclinical model that closely recapitulates the main characteristics of the primary tumor and could represent a useful asset to test new therapies. Here, using Positron Emission Tomography (PET) imaging, we verify how lung cancer PDXs reproduce the metabolic features of the corresponding primary tumors. **Methods:** We performed longitudinal ^{18}F-FDG-PET studies on nine different PDXs, obtained by implants of primary cancer fragments harvested from patients. Max ^{18}F-FDG uptake values of the lesion for each group were calculated and compared to corresponding patient's uptake. **Results:** Different PDXs showed variable tumor growth rate and ^{18}F-FDG uptake confirming the preservation of individual characteristics. A good intra-group reproducibility of PET measurements was observed. Furthermore, the subgroup of PDXs originating from primary tumors with higher metabolic rate displayed a rank order of ^{18}F-FDG uptake similar to that of patients' original SUV. **Conclusions:** PDXs reproduced the original glucose metabolism of primary lesions and represent therefore a promising preclinical model also for the early assessment of therapy efficacy.

INTRODUCTION

Lung cancer is a heterogeneous disease, characterized by poor outcome and limited response to pharmacological treatment. The expanding knowledge in genetics and molecular biology has led to reconsider the classical histological classification (*1*) suggesting personalized target-based and/or chemotherapeutic strategies according to the different molecular subtypes of tumors (*2,3*). Despite some efficacy in selected group of patients treated with epidermal growth factor receptor (EGFR) or anaplastic lymphoma kinase (ALK) inhibitors (*4-6*) this target-based approach has only marginally increased overall survival of patients and treatment of lung cancer still represents a major challenge since the presence of multiple modified pathways and the occurrence of therapy induced mutations greatly limits treatment efficacy (*7*). Development of second-generation kinase inhibitors, multi-targets combination therapy and novel immune system stimulating drugs may represent a novel strategy to reduce treatment failure (*8*).

Among other determinants of chemoresistance, Cancer Stem Cells (CSC, defined as the subset of tumor cells endowed with greater tumor forming potential) have been suggested as another key factor in the limited efficacy of therapy, because of their intrinsic chemoresistance and ability to support tumor re-growth (*9,10*). Development of agents targeting critical steps in CSCs-deregulated pathways (i.e., Wnt, Notch, Hedgehog) holds promise as an innovative therapeutic approach (*11*). In this context we have previously shown that in lung cancer CD133+ cells endowed with stem-like properties are resistant to cisplatin treatment (*10*) and recently identified CD133+/CXCR4+/EpCAM- cells as metastasis initiating cells (*12*).

Considering the high heterogeneity of lung cancer, preclinical models which recapitulate the specific genetic and cellular features of primary tumors, represent a major need in the identification and development of anticancer drugs. PDXs, obtained by direct implant of tissue fragments in immunocompromised mice, are of particular interest because they retain morphology, architecture, and molecular signatures of the parental primary tumor more closely than *in vitro* established cell lines (*13-15*). PDXs have been used to identify specific determinants of therapeutic response (*16,17*) and even to predict response to treatments of individual tumors (*18-20*). We previously reported the generation of PDXs from non-small lung

cancer (NSCLC) which closely maintained biological features of the parental tumors, including histology, immunophenotype, resistance to platinum based therapy and content of CD133+ cancer stem cells (*21*) and demonstrated the potential of using PDX to investigate dynamics of CSCs during pharmacological treatment (*22*).

The potential of PDX models to also reproduce metabolic features of corresponding primary tumors has however not been investigated. This has important clinical implications since metabolic reprogramming is now recognized as an hallmark of cancer cells (*23*) and a number of preclinical and clinical studies indicate the *in vivo* imaging of the Warburg effect with ^{18}F-FDG as non-invasive surrogate marker for the early prediction of prognosis and assessment of response to pharmacological treatment, including targeted therapies (*24-26*). Even for screen-detected lung cancers, stratification of patients on the basis of ^{18}F-FDG uptake (quantified as maximum standardized uptake value, SUVmax) has been shown to have prognostic value (*27*). In particular, we observed that SUVmax<2.5 defined a homogeneous population of small size (median diameter 11 mm, range 5–16), stage Ia tumors with a 100% 5-years survival. On the contrary, SUVmax higher than 8 defined a group of mostly advanced cancers (only 8% stage Ia), whose 20% survival was indicative of a highly metastatic biologic profile (*27*).

Specific mutations can also influence metabolic activity and in particular mutation or over-expression in tyrosine kinase receptors, PI3K/Akt/mTOR, RAS/RAF/MAPK or LKB1 results in increased activation of downstream signaling pathways that participate to reprogramming of tumor cell metabolism and influence ^{18}F-FDG uptake (*28,29*).

To investigate if NSCLC PDXs could maintain the same metabolic features of parental tumors, we selected from our previously established NSCLC PDXs, those deriving from patients who underwent a pre-surgery ^{18}F-FDG PET measurement and compared the glycolytic feature of the model with that of the corresponding patient. Furthermore we assessed if other features of PDXs such as tumor engraftment, growth rate and content of CSC are associated with SUV index. PDXs originating from primary tumors with SUVmax values higher than 8 displayed a good correlation with patients' values underscoring the potential of using ^{18}F-FDG PET in PDXs during pre-clinical development of novel therapeutic approaches.

MATERIALS AND METHODS

Patient-derived xenografts establishment

The Internal Review and the Ethics Boards of Fondazione IRCCS Istituto Nazionale dei Tumori (Milan, Italy) approved this study and all subjects signed a written informed consent (*10*).Tumor specimens derived from patients who performed a pre-surgical ^{18}F-FDG PET study were selected for the study. Patients ^{18}F-FDG SUV values were maintained blind to researchers who participated to preclinical PET study.

Female CD1 nude or SCID mice (7-10 weeks of age) were purchased from Charles River Laboratories. Animals were kept under specific pathogen-free conditions, handled and maintained according to Institutional Animal Care and Use Committee ethical regulations of the Fondazione IRCCS Istituto Nazionale dei Tumori and IRCCS Ospedale San Raffaele. PDX models were established as previously described (*21*).

PET analysis and quantification

Groups of animals (n = 5/6 per group) weekly performed ^{18}F-FDG PET studies for a month starting with a tumor dimension consistent with preclinical PET spatial resolution (4-5 mm, at first PET scan tumor volume varied from 50 mm^3 to 139 mm^3). Animals were weekly monitored for weight loss and tumor growth with caliper (Volume = $(a \times b^2)/2$; a: long side, b: short side). PET analysis and quantification were previously described (*26*).

Tumor growth rate was calculated during exponential growth phase and was quantified using specific growth rate (SGR; 1/d) as following: $SGR = \ln(V_2/V_1)/(t_2-t_1)$ where V is tumor volume and t is time of measure (*30*) and then was correlated with ^{18}F-FDG uptake both expressed as SUVmax and tumor on background ratio. SGR has been evaluated during different time point frames to include only the linear part of the growth curve.

Measurement of CD133+ and CD133+/CXCR4+/EpCAM- cells on PDX

For the detection of CD133+ CSC and the disseminating CD133+/CXCR4+/EpCAM- subset, procedures were previously described (*10,12*).

Statistical analysis

Results are expressed as mean ± standard deviation (SD) or standard error of the mean (SEM) where indicated. Correlation (R^2) was performed using the parametric Pearson test (2-

tailed, 95% confidence interval, Graph Pad Prism software) and it was considered statistically significant when p<0.05. Linear regression was also calculated using Prism.

RESULTS

PDXs can be established from primary tumors with different clinicopathological characteristics and ^{18}F-FDG SUV values.

Nine different PDXs groups were evaluated during the study (Table 1). Seven PDXs derived from lung adenocarcinomas, one from a squamous cell carcinoma and one from a large cell carcinoma. Grafted tumors had different clinical stage (Stage IV n = 1, Stage IIIA n = 4, Stage IIB n = 2 and Stage IA n = 2), lymph node involvement (N2 n = 4, N1 n = 2, N0 n = 3) and heterogeneous content of CD133+ cancer stem cells (four had more than 15% CD133+ cells, 2 between 1% and 15% and 3 less than 1%). Different 'driver' mutations were also observed (2 PDX showed mutations in KRAS, 4 in LKB1 and 1 in ERBB2). PDX were heterogeneous also for time of latency (time from implant to presence of palpable lesion, from 11.6 to 61.7 days) and growth rate (SGR value from 0.05 to 0.13) (Table 2). All these data confirm the individual nature of single PDXs. In particular six PDXs originated from primary tumors showing ^{18}F-FDG SUV values higher than 8, but grafting was obtained also from lesions with SUV < 6. Two PDXs derived from primary tumors having ^{18}F-FDG uptake within 2.5 and 8 SUV values and one from a primary tumor with ^{18}F-FDG uptake < 2.5.

SUVmax value of PDXs shows a good reproducibility, intragroup homogeneity and intergroup heterogeneity.

Under PET examination, PDXs models showed variable glucose uptake (Table 2) which reflects the heterogeneity observed in lung cancer patients. In some PDX tumors, ^{18}F-FDG uptake was high and tumors well visible such as PDX LT128, LT187, LT66, LT120, in other cases uptake was low and cancer lesions were poorly detectable such as PDX LT73 (Fig. 1). During the experimental observation time mice weight remained stable and no other clinical or behavioral signs were observed with the exception of PDX138 which induced syndrome of cachexia at later time points (Supplemental Fig. 1). In some models (LT66, LT111, LT120, LT128 and LT138) necrosis was visible in PET images when tumors became bigger than 300

mm^3, but when evaluated for correlations at volumes of 150 mm^3 ^{18}F-FDG was homogeneously distributed within lesions.

Among the group of 'low metabolic' lesions, PDX LT215 (patient SUVmax = 4.5) displayed an abrupt and sudden increase in tumor volume after engraftment and ^{18}F-FDG uptake between the second and the third PET scan (from 66.1±35 to 137±57 mm^3; from 0.62±0.1 to 1.3±0.3 SUVmax) as showed in Figure 1. Interestingly this tumor had no nodal involvement at diagnosis, but was associated with a synchronous brain metastasis.

To evaluate the influence of serial passages in the murine host on tumor metabolism we evaluated ^{18}F-FDG uptake in the same PDX model (LT66) at two different serial passages (p18 and p34). LT66p18 and LT66p34 displayed a similar rate of growth (data not shown) and similar values of ^{18}F-FDG uptake (p18: SUVmax = 1.27±0.15 for tumor volume of 874.40±273.18 mm^3 and; p34: SUVmax = 1.28±0.14 for tumor volume of 785.42±303.21 mm^3) (Fig. 2A). Regarding the possibility of necrosis, we observed a general but not continuous increase after p10 with comparable amounts of necrotic areas, slightly higher than primary tumor but similar to each other.

Intra models metabolic variability was in general low except for LT128 and LT187 (Fig. 2B; Supplemental fig. 2) which displayed a bimodal distribution. In both cases, half animals analyzed showed a higher ^{18}F-FDG uptake which could reflect different cell populations of the primary tumors.

Correlation of ^{18}F-FDG uptake with clinic pathological characteristics of tumors

Association analysis showed that neither tumor growth rate nor CD133+ CSC content were related with ^{18}F-FDG SUVmax or deltaSUVmax (Figs. 3A and 3B and data not shown). A slight positive correlation was however observed in PDXs between SUVmax and relative content of disseminating CSCs (CD133+/CXCR4+/EpCAM-) within the CSC pool when outliers (> 6 %) were removed (r = 0.79, p = 0.06).

Finally, by comparing ^{18}F-FDG uptake in lung cancer PDXs to that of the corresponding primary lesions, no statistical correlation was found when we considered the whole group of PDX (Fig. 4A). In detail, the three PDXs deriving from patients with SUV value < 8 and with absence of nodal involvement (N=0) failed to maintain the rank order of ^{18}F-

FDG uptake of corresponding primary lesions (Table 3). On the contrary, the PDXs deriving from the remaining subgroup of patients (lymph nodes positive and with SUV>8 in primary tumor), showed a trend of glucose metabolism similar to that observed in patients (R^2=0.72, p<0.05) (Fig. 4B).

DISCUSSION

The feasibility of an early evaluation of the efficacy of a treatment is of fundamental importance for the clinical management of patients. At present ^{18}F-FDG PET represents an interesting and foreseeing tool for the early assessment of drug efficacy (*25,31*). PDXs reproduce the patient's primary tumor for both immunohistochemical markers and genetic alterations as well as the maintenance of cellular heterogeneity (*20,21*).

Here, using PET imaging we evaluated glucose metabolism of PDX models of lung cancers derived by NSCLC patients with different clinic-pathological characteristics who underwent ^{18}F-FDG PET. PDX models were highly heterogeneous for growth rates and glycolytic features. Indeed, genetic modifications and rearrangements in some genes like as ALK, EGFR, KRAS, ERBB2, LKB1 could influence ^{18}F-FDG uptake. Recently, Choi et al. observed that patients with ALK-rearranged lung cancer showed higher glucose metabolism compared with wild type cases or those with EGFR mutation (*32*). In other tumor types, mutations in KRAS/BRAF or in LKB1 are in general related with an high glycolic phenotype (*29,33,34*).

Among our highly glycolytic tumors, PDX LT128 and PDX LT66 displayed mutations both in KRAS gene (c.34G>T) and in LKB1 gene (c.920+2T>A and c.298C>T respectively) which could partially explain the high ^{18}F-FDG uptake. Also, LT73 and LT138 showed mutations in LKB1 gene (c.859A>T, c.354delC respectively) but not in KRAS gene and displayed different SUVmax values. The correlation between specific gene alterations and glycolytic phenotype should therefore be investigated in greater detail potentially taking into account interactions among multiple mutations.

By comparing ^{18}F-FDG uptake of tumor in mice with the corresponding parental tumor, we observed that models derived by a neoplastic mass with a SUVmax value more than

8 showed the same ^{18}F-FDG uptake behavior of that of patients. This subgroup reproduces higher glycolytic tumors related with an higher metastatic potential and a worst prognosis in screen-detected lung cancer (*27*) (Fig. 4B). For such group of patients, identification and development of pharmacological treatment remains an unmet clinical need. In our previous study, glycolytic phenotype of tumor cells influenced response to VEGF-targeted treatment and the acquisition of resistance which could be monitored by PET imaging (*26*). In this context, metabolic alterations could be an interesting target for novel therapeutic approaches (*26,34*).

The three patients grafts with pre-surgical SUV < 8 didn't correlate with corresponding PDX SUV. Among these, two derived from low stage tumors (IA), one of which carrying an LKB1 mutation (c.354delC). The third PDX (LT215) derived from a patient who developed a small primary tumor (T2) with a SUVmax of 4.5, no evidences of lymph nodes involvement but synchronous brain metastasis. This PDX displayed a sudden and an abrupt increase of tumor volume and ^{18}F-FDG uptake possibly reflecting the aggressiveness of the parental primary tumor. In this case, we hypothesized that in the early phases of engraftment, when lesion size was smaller, tumor recapitulated glucose metabolism of the primary cancer lesion and then possibly a subpopulation of cells with a more aggressive phenotype already present in the original lesion took over during tumor growth (Fig. 1). As previously stated, ^{18}F-FDG uptake values of PDXs deriving from poorly glycolytic primary tumors with absence of nodal involvement failed to maintain the glycolytic phenotype of the original lesions (Fig. 4A and Table 3). Considering that such type of PDX has in general more difficulties to engraft (data not showed), we supposed that a selection of more resistant cells with a higher glucose metabolism might have supported the engraftment.

Concerning model reproducibility we observed that ^{18}F-FDG uptake, measured during the exponential phase after engraftment and at comparable tumor size, was homogenous within the same PDX group with the exception of LT128 and LT187 which showed similar although bimodal metabolic behavior which could reflect different cell populations of the parental tumors. In our platform of 38 lung cancer PDXs we have consistently observed that PDXs maintain primary tumor characteristics (histology, main histological patterns, marker expression, genetic profile, stromal content, necrosis amount and stem cell content) for several

passages in animal (>p10) (*21*). In the single case analyzed in this study, we observed the same metabolic features, independently of the number of passages. PDX are generated by subcutaneous implant in mice of a small fragments of primary tumor and after the first engraftment, reduced into fragment and transferred to other animals. Considering this possible source of variability, while a certain intra-lesion variability could sometimes be observed, the intragroup reproducibility of the measurements observed in our study was remarkable.

As previously indicated, PDXs recapitulated biological feature of corresponding clinical specimens including the content of CD133^{+} cancer stem cells or resistance to platinum therapy (*10,21*). While stemness properties are closely related to chemoresistance features, the low number of CSCs within primary tumor bulks makes it difficult to use CSCs markers in clinical practice and their visualization by molecular imaging is a challenging endeavor (*35*). As also observed by Gaedicke et al, we didn't find any correlation between CD133 expression and glucose metabolism as measured by ^{18}F-FDG uptake (*36*). In the same study the imaging of CD133+ cells could in fact only be obtained using a specific ^{64}Cu conjugated antibody-based tracer. However we observed a tendency for tumors with higher SUV to have a greater relative content of disseminating CSCs (CD133/CXCR4/EpCAM-), which we recently identified as being modulated by microenvironmental cues and related to bad clinical outcome in NSCLC patients (*12*). This could indicate a propensity for tumors with high glycolytic activity to induce selective enrichment of CSCs with disseminating ability, possibly providing a link between high SUV and worst prognosis.

Improved imaging of CSC with different strategies will be needed to evaluate the potential clinical relevance of CSCs tracking. In a recent study, in a mouse colon carcinoma (colon-26) tumor model, Yoshii et al. observed high uptake of ^{64}Cu-ATSM within regions with a high density of CD133 positive cells whereas regions with high uptake of ^{18}F-FDG had the lowest presence of CD133 positive cells (*37*). Moreover, in mice implanted with Lewis lung carcinoma (LLC1) tumor cells, Oh et al. found ^{64}Cu-ATSM accumulation in tumor regions composed by quiescent but clonogenic tumor cells with low glucose metabolism (*38*). Altogether these evidences suggest the use of specific tracers identifying a relative quiescence and low metabolic activity of CSC subset can be more useful than ^{18}F-FDG to CSC

subpopulation and could be implemented in association with PET to gain more information of tumor response during treatment.

CONCLUSION

In conclusion we show here that lung PDXs from primary tumor with SUVmax higher than 8, besides mirroring the histological phenotype and CSC content of the original tumor also maintain the same metabolic activity suggesting that these models may be more useful for more aggressive tumors with higher levels of metabolism. The combined use of PDXs and metabolic imaging could therefore represent a powerful preclinical tool for drug discovery and testing.

REFERENCES

1. Herbst RS, Heymach JV, Lippman SM. Lung cancer. *N Engl J Med.* 2008;359:1367-1380.

2. Politi K, Herbst RS. Lung cancer in the era of precision medicine. *Clin Cancer Res.* 2015;21:2213-2220.

3. Thomas A, Liu SV, Subramaniam DS, Giaccone G. Refining the treatment of NSCLC according to histological and molecular subtypes. *Nat Rev Clin Oncol.* 2015;12:511-26.

4. Shaw AT, Kim DW, Nakagawa K, et al. Crizotinib versus chemotherapy in advanced ALK-positive lung cancer. *N Engl J Med.* 2013;368:2385-2394.

5. Shepherd FA, Rodrigues Pereira J, Ciuleanu T, et al. Erlotinib in previously treated non-small-cell lung cancer. *N Engl J Med.* 2005;353:123-132.

6. Thatcher N, Chang A, Parikh P, et al. Gefitinib plus best supportive care in previously treated patients with refractory advanced non-small-cell lung cancer: results from a randomised, placebo-controlled, multicentre study (Iressa Survival Evaluation in Lung Cancer). *Lancet.* 2005;366:1527-1537.

7. Lovly CM, Shaw AT. Molecular pathways: resistance to kinase inhibitors and implications for therapeutic strategies. *Clin Cancer Res.* 2014;20:2249-2256.

8. Zhao Y, Adjei AA. New strategies to develop new medications for lung cancer and metastasis. *Cancer Metastasis Rev.* 2015;34:265-275.

9. Eramo A, Lotti F, Sette G, et al. Identification and expansion of the tumorigenic lung cancer stem cell population. *Cell Death Differ.* 2008;15:504-514.

10. Bertolini G, Roz L, Perego P, et al. Highly tumorigenic lung cancer CD133+ cells display stem-like features and are spared by cisplatin treatment. *Proc Natl Acad Sci U S A.* 2009;106:16281-16286.

11. Takebe N, Harris PJ, Warren RQ, Ivy SP. Targeting cancer stem cells by inhibiting Wnt, Notch, and Hedgehog pathways. *Nat Rev Clin Oncol.* 2011;8:97-106.

12. Bertolini G, D'Amico L, Moro M, Landoni E, Perego P, Miceli M. Microenvironment-modulated metastatic CD133+/CXCR4+/EpCAM- lung cancer-initiating cells sustain tumor dissemination and correlate with poor prognosis. *Cancer Res.* 2015;75:3636-3649.

13.   Tentler JJ, Tan AC, Weekes CD, et al. Patient-derived tumour xenografts as models for oncology drug development. *Nature Rev Clin Oncol.* 2012;9:338-350.

14.   Daniel VC, Marchionni L, Hierman JS, et al. A primary xenograft model of small-cell lung cancer reveals irreversible changes in gene expression imposed by culture in vitro. *Cancer Res.* 2009;69:3364-3373.

15.   Hao C, Wang L, Peng S, et al. Gene mutations in primary tumors and corresponding patient-derived xenografts derived from non-small cell lung cancer. *Cancer Lett.* 2015;357:179-185.

16.   Bertotti A, Migliardi G, Galimi F, et al. A molecularly annotated platform of patient-derived xenografts ("xenopatients") identifies HER2 as an effective therapeutic target in cetuximab-resistant colorectal cancer. *Cancer Discov.* 2011;1:508-523.

17.   Krumbach R, Schuler J, Hofmann M, Giesemann T, Fiebig HH, Beckers T. Primary resistance to cetuximab in a panel of patient-derived tumour xenograft models: activation of MET as one mechanism for drug resistance. *Eur J Cancer.* 2011;47:1231-1243.

18.   Hidalgo M, Bruckheimer E, Rajeshkumar NV, et al. A pilot clinical study of treatment guided by personalized tumorgrafts in patients with advanced cancer. *Mol Cancer Ther.* 2011;10:1311-1316.

19.   Dong X, Guan J, English JC, et al. Patient-derived first generation xenografts of non-small cell lung cancers: promising tools for predicting drug responses for personalized chemotherapy. *Clin Cancer Res.* 2010;16:1442-1451.

20.   Fichtner I, Rolff J, Soong R, et al. Establishment of patient-derived non-small cell lung cancer xenografts as models for the identification of predictive biomarkers. *Clin Cancer Res.* 2008;14:6456-6468.

21.   Moro M, Bertolini G, Tortoreto M, Pastorino U, Sozzi G, Roz L. Patient-derived xenografts of non small cell lung cancer: resurgence of an old model for investigation of modern concepts of tailored therapy and cancer stem cells. *J Biomed Biotechnol.* 2012;2012:568567-568577.

22.   Moro M, Bertolini G, Pastorino U, Roz L, Sozzi G. Combination treatment with all-trans retinoic acid prevents cisplatin-induced enrichment of CD133+ tumor-initiating cells and

reveals heterogeneity of cancer stem cell compartment in lung cancer. *J Thorac Oncol.* 2015;10:1027-1036.

23.   Ward PS, Thompson CB. Metabolic reprogramming: a cancer hallmark even warburg did not anticipate. *Cancer Cell.* 2012;21:297-308.

24.   Behzadi A, Ung Y, Lowe V, Deschamps C. The role of positron emission tomography in the management of non-small cell lung cancer. *Can J Surg.* 2009;52:235-242.

25.   van Gool MH, Aukema TS, Hartemink KJ, Valdes Olmos RA, van Tinteren H, Klomp HM. FDG-PET/CT response evaluation during EGFR-TKI treatment in patients with NSCLC. *World J Radiol.* 2014;6:392-398.

26.   Curtarello M, Zulato E, Nardo G, et al. VEGF-targeted therapy stably modulates the glycolytic phenotype of tumor cells. *Cancer Res.* 2015;75:120-133.

27.   Pastorino U, Landoni C, Marchiano A, et al. Fluorodeoxyglucose uptake measured by positron emission tomography and standardized uptake value predicts long-term survival of CT screening detected lung cancer in heavy smokers. *J Thorac Oncol.* 2009;4:1352-1356.

28.   Cairns RA, Harris IS, Mak TW. Regulation of cancer cell metabolism. *Nat Rev Cancer.* 2011;11:85-95.

29.   Kawada K, Nakamoto Y, Kawada M, et al. Relationship between ^{18}F-fluorodeoxyglucose accumulation and KRAS/BRAF mutations in colorectal cancer. *Clin Cancer Res.* 2012;18:1696-1703.

30.   Mehrara E, Forssell-Aronsson E, Ahlman H, Bernhardt P. Specific growth rate versus doubling time for quantitative characterization of tumor growth rate. *Cancer Res.* 2007;67:3970-3975.

31.   Nishiyama Y, Yamamoto Y, Kanenishi K, et al. Monitoring the neoadjuvant therapy response in gynecological cancer patients using FDG PET. *Eur J Nucl Med Mol Imaging.* 2008;35:287-295.

32.   Choi H, Paeng JC, Kim DW, et al. Metabolic and metastatic characteristics of ALK-rearranged lung adenocarcinoma on FDG PET/CT. *Lung Cancer.* 2013;79:242-247.

33.   Shackelford DB, Vasquez DS, Corbeil J, et al. mTOR and HIF-1alpha-mediated tumor metabolism in an LKB1 mouse model of Peutz-Jeghers syndrome. *Proc Natl Acad Sci U S A.* 2009;106:11137-11142.

34.   Nardo G, Favaro E, Curtarello M, et al. Glycolytic phenotype and AMP kinase modify the pathologic response of tumor xenografts to VEGF neutralization. *Cancer Res.* 2011;71:4214-4225.

35.   Xia T, Jiang H, Li C, Tian M, Zhang H. Molecular imaging in tracking tumor stem-like cells. *J Biomed Biotech.* 2012;2012:420364.

36.   Gaedicke S, Braun F, Prasad S, et al. Noninvasive positron emission tomography and fluorescence imaging of CD133+ tumor stem cells. *Proc Natl Acad Sci U S A.* 2014;111:E692-701.

37.   Yoshii Y, Furukawa T, Kiyono Y, et al. Copper-64-diacetyl-bis (N4-methylthiosemicarbazone) accumulates in rich regions of CD133+ highly tumorigenic cells in mouse colon carcinoma. *Nucl Med Biol.* 2010;37:395-404.

38.   Oh M, Tanaka T, Kobayashi M, et al. Radio-copper-labeled Cu-ATSM: an indicator of quiescent but clonogenic cells under mild hypoxia in a Lewis lung carcinoma model. *Nucl Med Biol.* 2009;36:419-426.
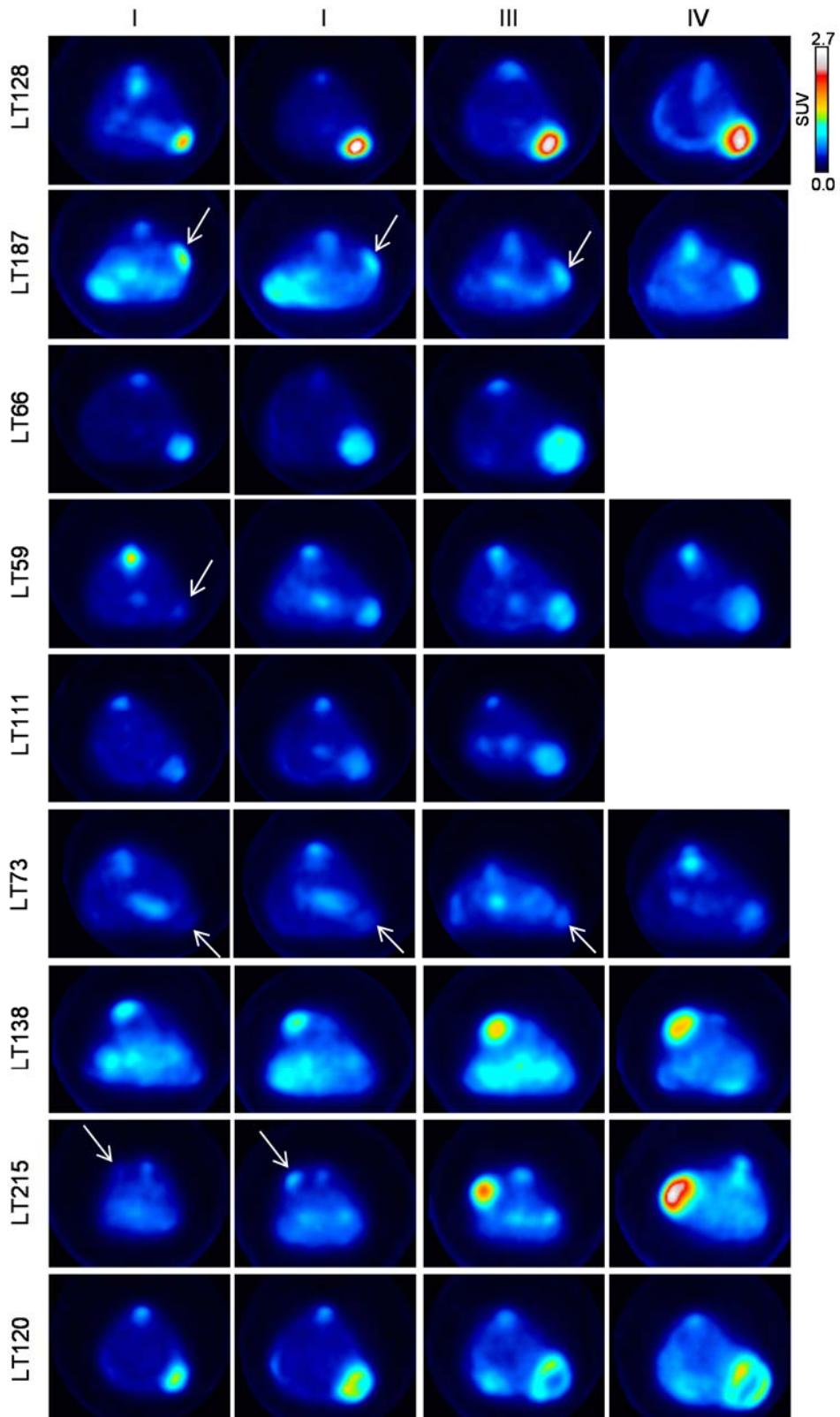
Figure 1

Figure 1: Representative PDX mice. Longitudinal images of ^{18}F-FDG PET scans of a representative patient-derived mouse for each group, intravenously injected with 4.2±0.3 MBq in overnight fasting conditions. White arrows indicate tumors. Color scale is expressed as SUV value.
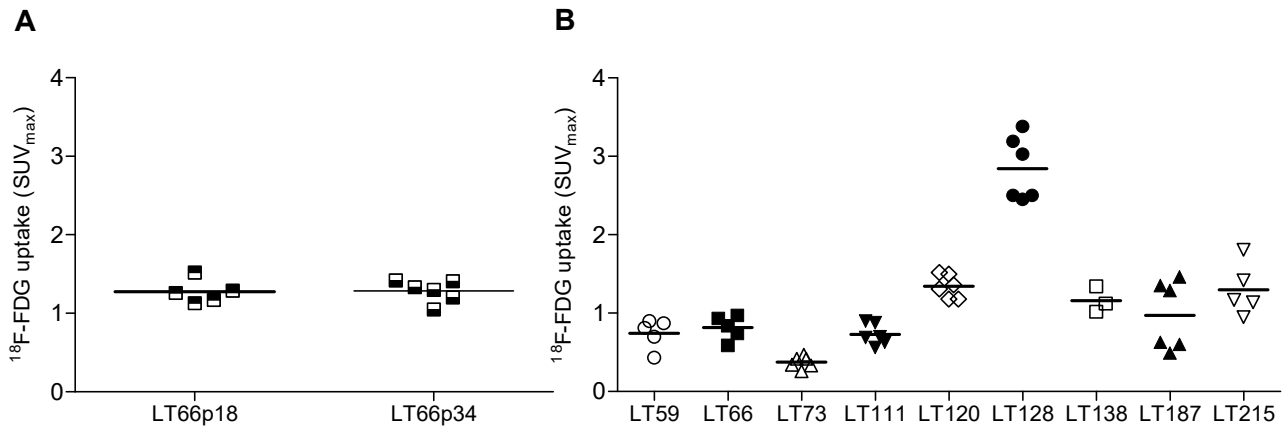
Figure 2

Figure 2: PDX PET characterization. (A) Distribution of ^{18}F-FDG uptake, expressed as SUVmax, in LT66 PDX model with similar tumor dimension (about 800 mm^2) after 18 and 34 in vivo passages. (B) Measurement of ^{18}F-FDG tracer uptake in multiple exponentially growing PDXs.
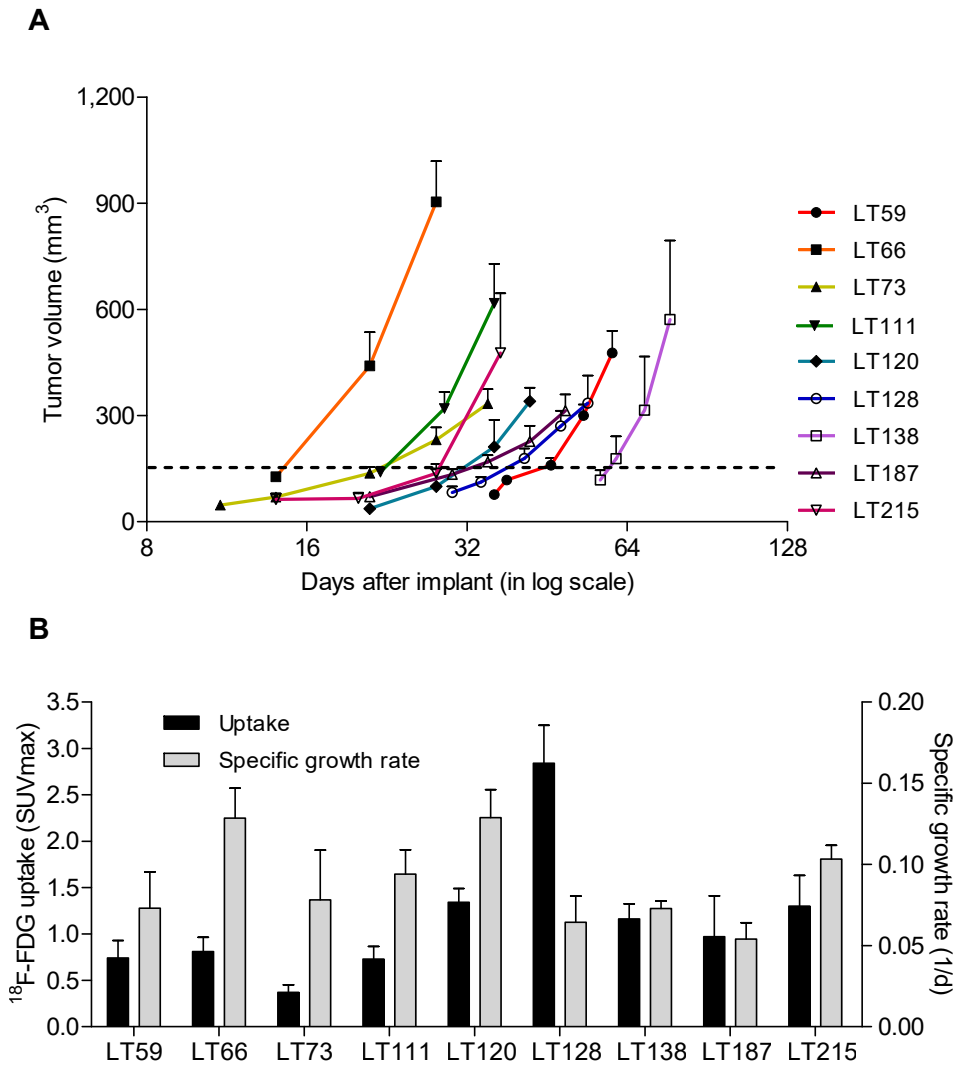
Figure 3

A

B

Figure 3: Correlation between tumor growth rate and ^{18}F-FDG uptake. (A) Tumor growth rate in the different PDX models (n=4-6 per each group). Error bars express SEM. (B) Tumor growth rate didn't reflect ^{18}F-FDG uptake in tested PDX. Error bars express SD.
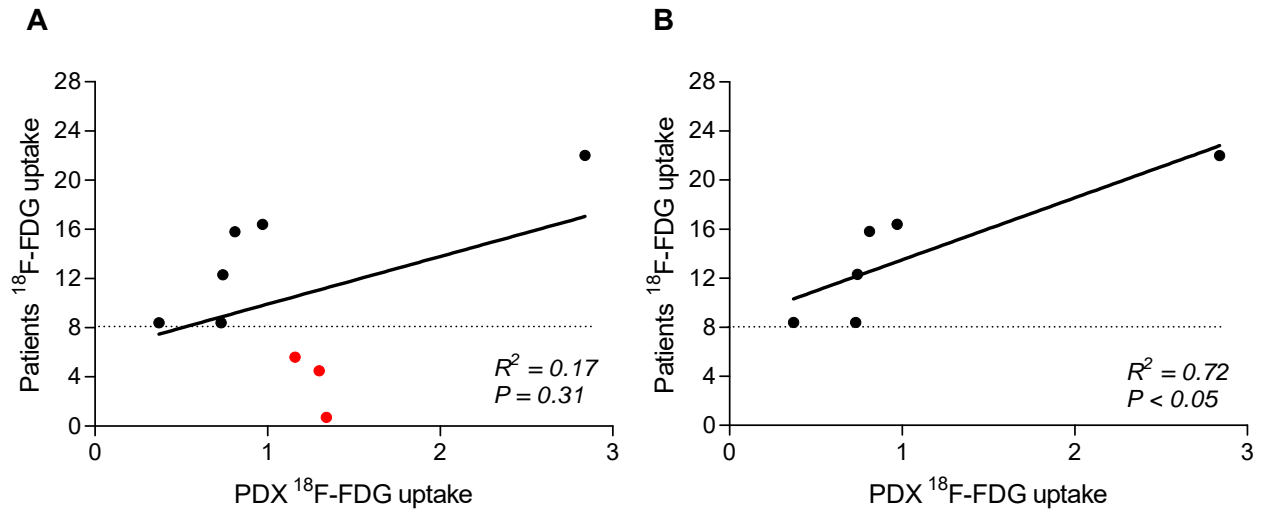
Figure 4

Figure 4: Glucose metabolism correlation between patients and corresponding PDX. (A) No correlation between primary tumors of patients and the corresponding PDX models was observed. (B) Excluding PDXs deriving from patients with SUV value < 8 (red points) a significant correlation was found. Even eliminating the highest SUV point, R^2 value remained good (R^2=0.62). ^{18}F-FDG uptake is expressed as SUVmax.

Table 1: summary of patients features

Patient	Tumor subtype	pStage	TNM	Grading	Tumor dimension (cm)	CD133+*	^{18}F-FDG SUV
LT128	ADC	IIIA	T2N2M0	G3	5.5	2	22.0
LT187	SCC	IIIA	T3N2M0	G3	7.0	nd	16.4
LT66	ADC	IIIA	T1N2M0	G3	1.9	0.2	15.8
LT59	LCC	IIIA	T1N2M0	G3	2.7	2	12.3
LT111	ADC	IIB	T2N1M0	G3	5.0	15	8.4
LT73	ADC	IIB	T2N1M0	G2	4.0	20	8.4
LT138	ADC	IA	T1N0M0	G3	1.3	nd	5.6
LT215	ADC	IV	T2N0M1	G3	4.0	nd	4.5
LT120	ADC	IA	T1N0M0	G1	1.5	23	0.7

pStage: pathologic stage; LCC: large cell carcinoma; ADC: adenocarcinoma; SCC: squamous cell carcinoma.

nd: not determined

*expressed as percentage

Table 2: summary of PDXs features

PDX	Latency#	SGR	CD133+*	CD133+ CXCR4+ EpCAM- °	KRAS (G12C)	LKB1	^{18}F-FDG SUV
LT128	34.3±5.4	0.06±0.02	1.5	4.8	mut	(c.920+2T>A)	2.84±0.41
LT187	29.3±3.1	0.05±0.01	0.2	6	wt	wt	0.97±0.44
LT66	11.6±1.3	0.13±0.02	0.5	nd	mut	c.298C>T	0.81±0.15
LT59	38.8±3.1	0.07±0.02	85	0.8	wt	wt	0.74±0.19
LT111	17.8±2.0	0.09±0.01	15	2	wt	wt	0.73±0.14
LT73	18.3±2.6	0.08±0.03	3	0.5	wt	c.859A>T	0.37±0.08
LT138	61.7±8.1	0.07±0.00	85	0.3	nd	c.354delC	1.16±0.16
LT215	25.8±7.4	0.10±0.01	0.2	4	nd	wt	1.30±0.33
LT120	25.0±6.2	0.13±0.02	30	95	nd	nd	1.34±0.15

\# expressed as days

* expressed as percentage

° expressed as percentage within CD133+ cells

wt: wild type; SGR: specific growth rate; nd: not determined

Latency, SGR and ^{18}F-FDG are expressed as mean ± SD (n=3/6 animals per each group).

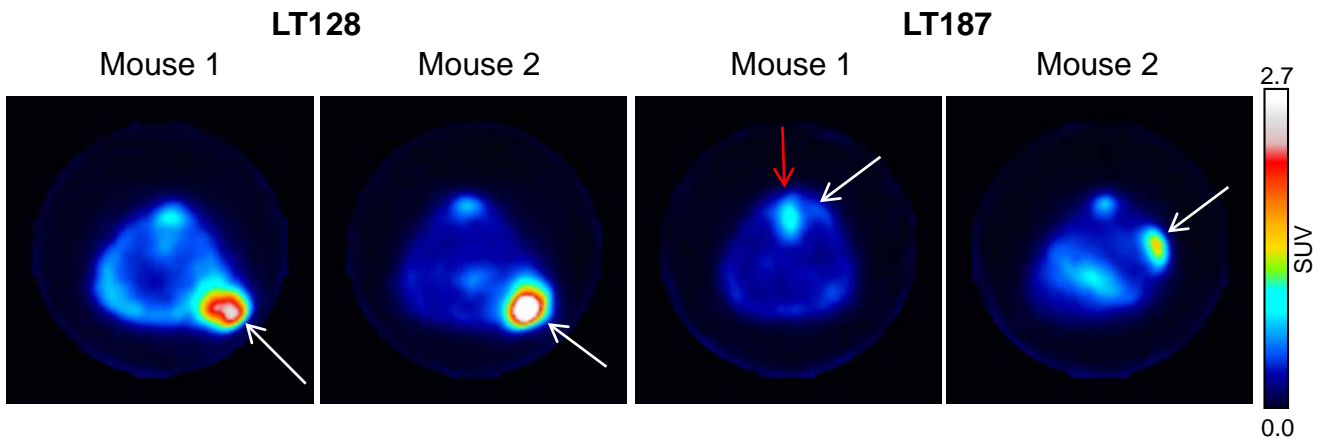**Table 3:** comparison between patients and PDXs ^{18}F-FDG uptake (SUVmax)

Groups	Patients	PDX
LT128	22	2.84
LT187	16.4	0.97
LT66	15.8	0.81
LT59	12.3	0.74
LT111	8.4	0.73
LT73	8.4	0.37
LT138	5.6	1.16
LT215	4.5	1.30
LT120	0.7	1.34

Supplemental Figure 1
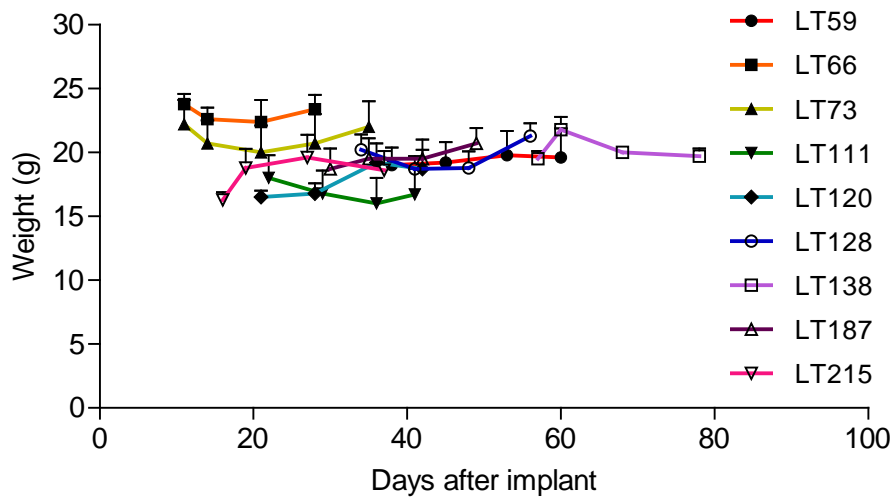
Graph of animals weight measured during the observed period.

Supplemental Figure 2

| LT128 | | LT187 | |
| Mouse 1 | Mouse 2 | Mouse 1 | Mouse 2 |

Trans axial images of ^{18}F-FDG PET scans of two representative LT128 and LT187 mice with same tumor dimension but different uptake. Color scale is expressed as SUV value. White arrows indicate lesion whereas red arrow indicates nonspecific uptake.